Correspondence to:
J. Li,
jun.li@ssec.wisc.edu

An efficient radiative transfer model for hyperspectral IR radiance simulation and applications under cloudy-sky conditions

Jun Li[1] (iD), Zhenglong Li[1] (iD), Pei Wang[1] (iD), Timothy J. Schmit[2] (iD), Wenguang Bai[3], and Robert Atlas[4] (iD)

[1]Cooperative Institute for Meteorological Satellite Studies, University of Wisconsin-Madison, Madison, Wisconsin, USA, [2]ASPT/CoRP, Center for Satellite Applications and Research, Madison, Wisconsin, USA, [3]National Satellite Meteorological Center, China Meteorological Administration, Beijing, China, [4]Atlantic Oceanographic and Meteorological Laboratory, NOAA, Miami, Florida, USA

Abstract An efficient radiative transfer model has been developed for hyperspectral infrared radiance simulation under both clear- and cloudy-sky conditions. The hyperspectral IR cloudy radiative transfer model (HIRTM) combines atmospheric transmittances due to molecular absorption and cloud absorption and scattering from cloud hydrometeors. An efficient analytical Jacobian methodology is also developed under both clear- and cloudy-sky conditions, which is needed both to assimilate cloudy radiances directly into numerical weather prediction models and to retrieve atmospheric soundings and cloud properties simultaneously from cloudy radiance measurements. In comparing HIRTM and its analytical Jacobian with the community radiative transfer model (CRTM), our research has shown that HIRTM's Jacobian calculations are similar to those of CRTM. HIRTM and CRTM synthetic observations derived from model output are compared with corresponding real observations from Geostationary Operational Environmental Satellite 13 Imager observations, and both perform similarly under water clouds, while CRTM is colder than HIRTM for thick ice clouds.

1. Introduction

Hyperspectral infrared (IR) sounder radiance measurements from satellites have started a new era of global atmospheric sounding applications [*Smith et al.*, 2009]. Hyperspectral IR radiance observations from the Atmospheric Infrared Sounder (AIRS) [*Chahine et al.*, 2006], Cross-Track Infrared Sounder [*Gambacorta and Barnet*, 2013], and Infrared Atmospheric Sounder Interferometer [*Karagulian et al.*, 2010] have been widely used in operational numerical weather prediction (NWP) centers and play an important role in daily weather forecasts [*Le Marshall et al.*, 2005, 2006; *Kelly and Thepaut*, 2007; *Cardinali*, 2009]. While challenging, assimilating cloudy radiances in NWP is required to take full advantage of IR sounder thermodynamic and hydrometric information. Usually, only IR radiances from a clear field-of-view or clear IR channels (not affected by clouds) are used in data assimilation. In regions with extensive cloud cover, this approach can drastically reduce the potential impact. Cloud contaminated channels have not been used effectively due to challenges in modeling clouds in both the NWP forecast and radiative transfer models [*Li et al.*, 2016]. This is one reason why NWP analysis and forecasts have larger errors in cloudy regions than in clear skies. Cloud-clearing techniques can derive clear equivalent radiances by combining the collocated advanced IR sounder data with the advanced microwave sounder data [*Susskind et al.*, 2003] or combining the collocated advanced IR sounder data with the high spatial resolution imager data [*Li et al.*, 2005] together. However, NWP centers have identified the direct assimilation of advanced IR sounder cloudy radiances through a radiative transfer model (RTM) accounting for clouds as a requirement for progress in radiance assimilation. This process brings cloud information into NWP analyses which should reduce errors in cloudy regions.

Improving the application of cloudy radiances in NWP depends on a reliable cloudy radiative transfer (RT) model. Community radiative transfer model (CRTM) and (Radiative Transfer for Television and Infrared Observation Satellite (TIROS) Operational Vertical Sounder) (RTTOV) are two typical RT models currently used by many operational centers for data assimilation. RTTOV (http://research.metoffice.gov.uk/research/inter-proj/nwpsaf/rtm/rttov9_files/users_guide_9_v1.7.pdf) provides two options for handling clouds: (a) cloud top pressure and effective cloud amount can be specified for simple, single-layer cloudy radiance

calculations, and (2) a full cloud water/ice profile can be supplied for cloudy radiance simulation with various overlap assumptions. In the second option, a multiple scattering radiance simulation scheme has been developed with improved accuracy in multilayer clouds, but the calculation is too slow for real-time applications. In CRTM, the cloud absorption and scattering module calculates cloud optical parameters, such as the mass extinction coefficient, single-scattering albedo, asymmetric factor, and Legendre phase coefficients. For IR sensors, the spectral optical properties of the spherical particles used for liquid clouds and the mixed ice crystal habits for ice and hail clouds are provided by Texas A&M University [*Yang et al.*, 1997; *Wei et al.*, 2004].

Even with these existing RT models, direct assimilation of IR cloudy radiances is still challenging due to the fact that (1) both NWP and RTM have larger uncertainties in cloudy regions, (2) there is a significant change in the temperature Jacobians at cloud level (assuming level clouds instead of layers), (3) satellite observations and NWP may be inconsistent on clouds (e.g., the satellite has clouds but NWP does not and vice versa), and (4) atmospheric parameters have a higher nonlinearity to the IR radiances in cloudy situations [*Li et al.*, 2016]. Alternative approaches for cloudy radiative transfer calculations are desired in order to conduct intercomparisons between different models, which can lead to better uncertainty quantification and improved applications.

In this study, an efficient hyperspectral IR radiative transfer calculation along with an analytical Jacobian method under cloudy-sky conditions is developed. This hyperspectral IR RTM (HIRTM) couples the atmospheric molecular absorption and cloud scattering. It is different from the simple cloudy RTM model based on a geometry assumption which uses effective cloud top height and effective cloud amount (or effective cloud emissivity). In HIRTM, the cloudy portion is based on cloud scattering and absorption model, which is based on effective cloud top height, cloud phase, particle size, and optical thickness. However, there is a link between the simple geometry model and HIRTM since the effective cloud amount is a function of cloud particle size and optical thickness, which has been described by *Heilliette and Garand* [2007].

HIRTM has been successfully utilized for many applications, such as extracting products of atmospheric profiles and cloud properties [*Li et al.*, 2005; *Zhou et al.*, 2007; *Li et al.*, 2008; *Smith et al.*, 2012; *Weisz et al.*, 2007, 2013; *Wu et al.*, 2005], real-time applications of those products in weather analysis [*Huang et al.*, 2004; *Weisz et al.*, 2007], nowcasting and forecasting [*Li et al.*, 2008, 2009; *Weisz et al.*, 2015], and climate research [*Smith et al.*, 2015]. In addition, HIRTM can be used for future observing system simulation [*Greenwald et al.*, 2016], evaluating NWP model forecasts by converting the forecasts to the simulated brightness temperatures (BTs) and comparing with BT observations [*Jiang*, 2016], as well as for evaluating microphysical schemes in a NWP model [*Cintineo et al.*, 2014]. This paper describes the method, which was developed at the University of Wisconsin-Madison but not previously documented, so that anyone using this model has detailed information for improved applications.

Section 2 introduces the radiative transfer calculation algorithm for cloudy-sky conditions; section 3 describes the analytical Jacobian under cloudy conditions which are needed for sounding/cloud retrieval and radiance assimilation. The comparisons between HIRTM and CRTM are given in sections 4 and 5. Summary and concluding remarks are given in section 6.

2. IR Radiative Transfer Calculation Algorithm Under Cloudy-Sky Conditions

In HIRTM, the atmospheric transmittance model is from the Stand-Alone Radiative Transfer Algorithm [*Hannon et al.*, 1996; *Strow et al.*, 2003] (see information online at http://asl.umbc.edu/pub/rta/sarta/), which has 100 pressure layers (101 pressure levels), with vertical coordinates from 0.005 to 1100 hPa. The computation takes into account the satellite zenith angle, absorption by well-mixed gases (including nitrogen and oxygen), water vapor (including the water vapor continuum), ozone, and carbon dioxide. It should be noted that the transmittance calculations only rely on the molecular absorption in the IR spectral region, but they can also be derived from other radiative transfer models. In the cloud absorption and scattering model, the bulk single-scattering properties of ice crystals are derived by assuming aggregates for large particles (300 μm), hexagonal geometries for moderate particles (50–300 μm), and droxtals for small particles (0–50 μm) [*Wei et al.*, 2004]. Spherical water droplets are assumed for water clouds, and the classical Lorenz-Mie theory is used to compute their single-scattering properties. In the model input, the cloud optical thickness (COT) is specified in terms of its visible optical thickness at 0.55 μm (τ_{vis}). The IR COT ($\tau(\lambda)$) for each IR channel can be derived through the following relationship:
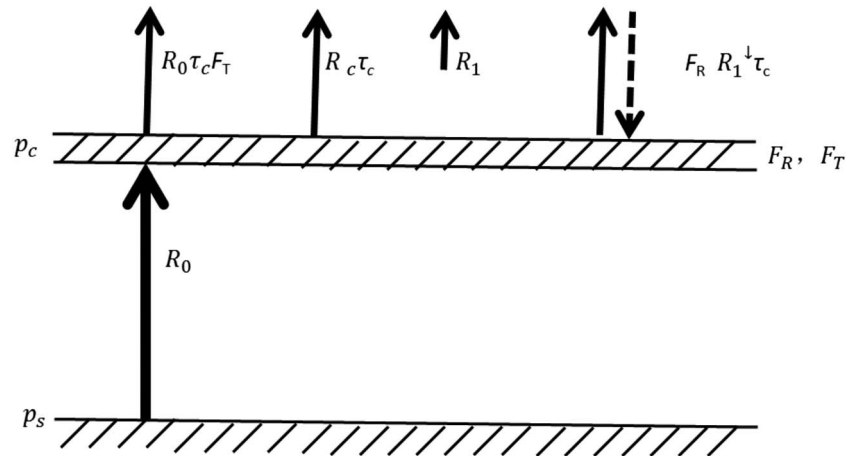
Figure 1. Diagram of an effective single-layer cloud assumption for IR radiative transfer 546 equation derivation.

$$\tau(\lambda) = \frac{<Q_e(\lambda)>}{2}\tau_{\text{vis}} \tag{1}$$

where $Q_e(\lambda)$ is the bulk mean extinction efficiency. Given the visible COT and cloud particle size (CPS) in diameter, the IR COT, the single-scattering albedo, and the asymmetry factor can be obtained from a prescribed parameterization of the bulk radiative properties of ice clouds and water clouds. The detailed parameterization scheme has been described by *Wei et al.* [2004]. The cloudy radiance for a given IR sounder or imager channel can be computed by coupling the clear-sky optical thickness and the cloud optical effects. The cloud optical effects are accounted for by using a precomputed lookup table of cloud reflectance and transmittance on the basis of fundamental radiative transfer principles; therefore, the radiative transfer equation in cloudy situations for a given IR channel can be derived for radiance simulation and applications.

It should be pointed out that this cloud model assumes effective single-layer clouds. While a multiple-layer cloud model is desired, its computational efficiency does not meet the requirement for real-time or near-real-time processing of hyperspectral sounder data, in both sounding retrievals and radiance assimilation. Based on previous work with this single-layer cloud model [*Li et al.*, 2009; *Smith et al.*, 2012], it is possible to simulate reasonable cloudy radiances over multiple-layer clouds. However, the difficulty is in how to estimate cloud top pressure from the NWP cloud profiles. More details on this issue will be provided in section 4. In addition, the regression coefficients derived using this single-layer cloud model can be used to retrieve cloud top pressure for thin cirrus over low water clouds [*Li et al.*, 2009].

Consider an effective single layer of clouds (see Figure 1) with the following definitions [*Zhou et al.*, 2007] used in the radiative transfer equation:

R_0	upwelling radiance at the base of clouds;
$R_0^{\downarrow}$	downwelling radiance at the surface;
R_c	radiance from clouds;
R_1	upwelling radiance above clouds;
$R_1^{\downarrow}$	downwelling radiance by the atmosphere at the top of clouds;
F_R	cloud reflectivity (albedo);
F_T	cloud transmittance;
$\tau_{(P)}$	atmospheric gas transmittance function $(0 - P)$;
τ_c	atmospheric transmittance of the cloud top $(0 - P_c)$;
τ_s	atmospheric transmittance of the surface $(0 - P_s)$;
P_c	effective cloud top pressure (CTP);
$B(P)$	Plank function as $T(P)$;
B_s	Planck function of the surface skin temperature;
B_c	Planck function of the cloud top temperature;
$\tau_b(P)$	transmittance function below cloud $(P_c - P)$.

$$\tau_b(P_c) = 1$$

$$\tau_b(P) = \frac{\tau(P)}{\tau_c}$$

For a given IR channel, the radiance reaching the satellite sensor can be described a

$$R = R_0 F_T \tau_c + R_c \tau_c + R_1 + R_1^{\downarrow} F_R \tau_c \tag{2}$$

where

$$R_1 = \int_{P_c}^{0} B d\tau$$

$$R_1^{\downarrow} = \int_{0}^{P_c} B d$$

$$R_c = (1 - F_T - F_R) B_c$$

Put $R, R_1, R_1^{\downarrow}$, and R_c into equation (2), we have

$$R = R_0 F_T \tau_c + (1 - F_T - F_R) B_c \tau_c + \int_{P_c}^{0} B d\tau + F_R \tau_c \int_{0}^{P_c} B d \frac{\tau_c}{\tau_{(P)}} \tag{3}$$

and

$$R_0 = \varepsilon_s B_s \tau_{bs} + \int_{P_s}^{P_c} B d\tau_b(P) + (1 - \varepsilon_s) \tau_{bs} R_0^{\downarrow} \tag{4}$$

$$R_0^{\downarrow} = \tau_{bs} \left(R_1^{\downarrow} F_T + R_c \right) + \int_{P_c}^{P_s} B d \frac{\tau_{bs}}{\tau_b(P)} \tag{5}$$

Combining equations (3) and (4), we have

$$R_0 = \varepsilon_s B_s \tau_{bs} + \int_{P_s}^{P_c} B d\tau_b(P) + (1 - \varepsilon_s) \tau_{bs} \left\{ \tau_{bs} \left[F_T \int_{0}^{P_c} B d \frac{\tau_c}{\tau_{(P)}} + (1 - F_T - F_R) B_c \right] + \int_{P_c}^{P_s} B d \frac{\tau_{bs}}{\tau_b(P)} \right\} \tag{6}$$

From equation (6), we have

$$R_0 = \varepsilon_s B_s \tau_{bs} + \int_{P_s}^{P_c} B d\tau_b(P) + (1 - \varepsilon_s) \tau_{bs}^2 F_T \int_{0}^{P_c} B d \frac{\tau_c}{\tau_{(P)}} + (1 - \varepsilon_s) \tau_{bs}^2 (1 - F_T - F_R) B_c + (1 - \varepsilon_s) \tau_{bs} \int_{P_c}^{P_s} B d \frac{\tau_{bs}}{\tau_b(P)} \tag{7}$$

Since $\tau_b(P) = \frac{\tau(P)}{\tau_c}$ and $\tau_{bs} = \frac{\tau_s}{\tau_c}$, equation (7) becomes

$$R_0 = \varepsilon_s B_s \frac{\tau_s}{\tau_c} + \int_{P_s}^{P_c} B d \frac{\tau(P)}{\tau_c} + (1 - \varepsilon_s) \frac{\tau_s^2}{\tau_c^2} F_T \int_{0}^{P_c} B d \frac{\tau_c}{\tau_{(P)}} + (1 - \varepsilon_s) \frac{\tau_s^2}{\tau_c^2} (1 - F_T - F_R) B_c + (1 - \varepsilon_s) \frac{\tau_s}{\tau_c} \int_{P_c}^{P_s} B d \frac{\tau_s}{\tau(P)} \tag{8}$$

Substituting equation (8) into equation (3), we have

$$R = R_0 F_T \tau_c + (1 - F_T - F_R) B_c \tau_c + \int_{P_c}^{0} B d\tau + F_R \tau_c \int_{0}^{P_c} B d \frac{\tau_c}{\tau_{(P)}}$$

$$= \varepsilon_s B_s \tau_s F_T + F_T \int_{P_s}^{P_c} B d\tau + (1 - \varepsilon_s) F_T^2 \int_{0}^{P_c} B d \frac{\tau_s^2}{\tau(P)} + (1 - \varepsilon_s) F_T \frac{\tau_s^2}{\tau_c} (1 - F_T - F_R) B_c + (1 - \varepsilon_s) F_T \int_{P_c}^{P_s} B d \frac{\tau_s^2}{\tau(P)}$$

$$+ (1 - F_T - F_R) B_c \tau_c + \int_{P_c}^{0} B d\tau + F_R \tau_c \int_{0}^{P_c} B d \frac{\tau_c}{\tau_{(P)}}$$

$$= \varepsilon_s B_s \tau_s F_T + F_T \int_{P_s}^{P_c} B d\tau + (1 - \varepsilon_s) F_T \int_{P_c}^{P_s} B d \frac{\tau_s^2}{\tau(P)} + (1 - F_T - F_R) \tau_c \left[(1 - \varepsilon_s) F_T \frac{\tau_s^2}{\tau_c^2} + 1 \right] B_c$$

$$+ (1 - \varepsilon_s) F_T^2 \int_{0}^{P_c} B d \frac{\tau_s^2}{\tau(P)} + F_R \int_{0}^{P_c} B d \frac{\tau_c^2}{\tau_{(P)}} + \int_{P_c}^{0} B d\tau \tag{9}$$

In clear skies $F_T = 1$, $F_R = 0$, equation (9) becomes

$$R = \varepsilon_s B_s \tau_s + \int_{P_s}^{0} B d\tau + (1 - \varepsilon_s) \int_{0}^{P_s} B d \frac{\tau_s^2}{\tau(P)} \tag{10}$$

This is a typical analytical IR radiative transfer equivalent form, which can be used to retrieve atmospheric profiles and surface IR emissivities in clear skies from radiance measurements of hyperspectral IR sounders such as AIRS [Li et al., 2007, 2008; Li and Li, 2008].

Define $\tau^*(P) = \frac{\tau_s^2}{\tau(P)}$, $\tilde{\tau}^*(P) = \frac{\tau_c^2}{\tau(P)}$, from equation (9), we have

$$R = \varepsilon_s B_s \tau_s F_T + F_T \int_{P_s}^{P_c} B d\tau + (1 - \varepsilon_s) F_T \int_{P_c}^{P_s} B d\tau^*(P) + (1 - F_T - F_R) \left(1 + F_T \frac{\tau_s^2}{\tau_c^2} - \varepsilon_s F_T \frac{\tau_s^2}{\tau_c^2} \right) B_c \tau_c$$

$$+ (1 - \varepsilon_s) F_T^2 \int_0^{P_c} B d\tau^*(P) + F_R \int_0^{P_c} B d \tilde{\tau}^*(P) + \int_{P_c}^0 B d\tau \qquad (11)$$

In equation (11), the first three terms reflect the atmospheric radiation below the clouds, the fourth term reflects the radiation from the cloud top, while the last three terms reflect the radiation above the clouds. The cloudy radiance for a given IR channel can be calculated if the cloud top pressure and the cloud transmissive (including both direct and diffuse parts) and reflective (or albedo) functions are provided. The HIRTM was developed based on equation (11).

3. Linearization of HIRTM Analytically Under Cloudy Skies

The analytical Jacobian in clear-sky conditions was developed [*Li*, 1994; *Li et al.*, 1994, 2000, 2008] for many real-time sounding applications. The Jacobians for cloud properties such as cloud top pressure were also developed for cloud product retrieval [*Li et al.*, 2001, 2004, 2005]. With the fast radiative transfer equation (RTE) calculation in equation (10), one can simulate radiances in real time; for example, the real-time NWP forecasts can be converted to simulated radiances and compared with radiance observations to verify and correct forecasts [*Cintineo et al.*, 2014; *Jiang*, 2016]. On the other hand, in order to derive the atmospheric cloud properties and sounding products, or assimilate radiances in real time, the linearization of the radiative transfer equation is needed. In this manuscript, efficient analytical Jacobians for temperature and moisture soundings are derived under cloudy conditions for any given IR channel.

For simplicity in linearizing equation (11), we assume that the surface IR emissivity is 1.0 for the last three terms in equation (11) above the clouds. Note that in the radiance calculations, the emissivity is not set to be 1.0; only in the Jacobian calculation (linearization of equation (11)) is the surface emissivity set to be 1.0 for the radiances above the clouds and penetrating the clouds. The surface radiation still uses the input emissivity (not 1.0). Therefore, the impact of emissivity on the Jacobian in cloudy situations should be negligible; doing this makes the analytical Jacobian much simpler. Therefore, the simplified RTE for linearization will be

$$R = \varepsilon_s B_s \tau_s F_T + F_T \int_{P_s}^{P_c} B d\tau + (1 - F_T - F_R) B_c \tau_c + F_R \int_0^{P_c} B d \tilde{\tau}*(P) \int_{P_c}^0 B d\tau$$

$$= \varepsilon_s B_s \tau_s F_T - F_T \int_0^{P_s} B d\tau + (1 - F_T - F_R) B_c \tau_c - (1 - F_T) \int_0^{P_c} B d\tau + F_R \int_0^{P_c} B d\tilde{\tau}* \qquad (12)$$

Define a generic form as below

$$\tau^* = \frac{\tau_s^2}{\tau(P)}$$

$$\tilde{\tau}^* = \frac{\tau_{P_c}^2}{\tau(P)}$$

$$R(P_s) = a(P_s) B_s \tau_s - b(P_s) \int_0^{P_s} B d\tau + c(P_s) \int_0^{P_s} B d\tau^* \qquad (13)$$

Equation (12) can be rewritten as

$$R = R(P_s) + R(P_c) \qquad (14)$$

where

$$a(P_s) = \varepsilon_s F_T$$
$$b(P_s) = F_T$$
$$c(P_s) = 0$$
$$a(P_c) = 1 - F_T - F_R$$
$$b(P_c) = 1 - F_T$$

$$c(P_c) = F_R$$

To linearize equation (13), take the variation on both sides of the equation so that

$$\delta R(P_s) = a(P_s)B_s\delta\tau_s + a(P_s)\delta B_s\tau_s - b(P_s)\int_0^{P_s}Bd\delta\tau - b(P_s)\int_0^{P_s}\delta Bd\tau + c(P_s)\int_0^{P_s}Bd\delta\tau^* + c(P_s)\int_0^{P_s}\delta Bd\tau^* \qquad (15)$$

Since

$$\int_0^{P_s}Bd\delta\tau = B_a\delta\tau_s - \int_0^{P_s}\delta\tau dB \qquad (16)$$

$$\int_0^{P_s}Bd\delta\tau^* = B_a\delta\tau_s - \int_0^{P_s}\delta\tau^*dB \qquad (17)$$

where B_a is Planck function of surface air temperature T_a. Substitute equations (16) and (17) into equation (15), we have

$$\delta R(P_s) = a(P_s)B_s\delta\tau_s + a(P_s)\tau_s\delta B_s - b(P_s)B_a\delta\tau_s + b(P_s)\int_0^{P_s}\delta\tau dB - b(P_s)\int_0^{P_s}\delta Bd\tau + c(P_s)B_a\delta\tau_s - c(P_s)\int_0^{P_s}\delta\tau^*dB$$
$$+ c(P_s)\int_0^{P_s}\delta Bd\tau^*$$

$$= a(P_s)\tau_s\delta B_s + [a(P_s)B_s - b(P_s)B_a + c(P_s)B_a]\delta\tau_s - \int_0^{P_s}\delta Bd(b(P_s)\tau - c(P_s)\tau^*) + b(P_s)\int_0^{P_s}\delta\tau dB$$
$$- c(P_s)\int_0^{P_s}\delta\tau^*dB \qquad (18)$$

Following *Li* [1994]

$$\delta\tau = \tau\int_0^P \delta\ln q d\ln\tau_w \qquad (19)$$

$$\delta\tau^* = 2\tau^*\int_0^{P_s}\delta\ln q d\ln\tau_w - \tau^*\int_0^P\delta\ln q d\ln\tau_w \qquad (20)$$

Substituting equations (19) and (20) into equation (18), we have

$$\delta R(P_s) = a(P_s)\tau_s\delta B_s + [a(P_s)B_s - b(P_s)B_a + c(P_s)B_a]\tau_s\int_0^{P_s}\delta\ln q d\ln\tau_w -$$
$$\int_0^{P_s}\delta Bd(b(P_s)\tau - c(P_s)\tau^*) + b(P_s)\int_0^{P_s}d\ln q\left[\int_P^{P_s}\tau dB\right]d\ln\tau_w +$$

$$c(P_s)\int_0^{P_s}\delta\ln q\left[\int_P^{P_s}\tau^*dB - 2\int_0^{P_s}\tau^*dB\right]d\ln\tau_w$$

$$= a(P_s)\tau_s\delta B_s + \int_0^{P_s}\delta Bd(b(P_s)\tau - c(P_s)\tau^*)$$

$$+\int_0^{P_s}\delta\ln q\left[(a(P_s)B_s - b(P_s)B_a + c(P_s)B_a)\tau_s + b(P_s)\int_P^{P_s}\tau dB + c(P_s)\left(\int_P^{P_s}\tau^*dB - 2\int_0^{P_s}\tau^*dB\right)\right]d\ln\tau_w$$

$$= a(P_s)\tau_s\frac{\partial B_s}{T_s}\delta T_s + \int_0^{P_s}\frac{\partial B}{\partial T}\delta Td(b(P_s)\tau - c(P_s)\tau^*) + \qquad (21)$$

$$\int_0^{P_s}\delta\ln q\left[(a(P_s)B_s - b(P_s)B_a + c(P_s)B_a)\tau_s + b(P_s)\int_P^{P_s}\tau dB + c(P_s)\left(\int_P^{P_s}\tau^*dB - 2\int_0^{P_s}\tau^*dB\right)\right]d\ln\tau_w$$

$$= a(P_s)\tau_s\frac{\partial B_s}{T_s}\delta T_s + \int_0^{P_s}\frac{\partial B}{\partial T}\left(b(P_s)\frac{\partial\tau}{\partial P} - c(P_s)\frac{\partial\tau^*}{\partial P}\right)\delta TdP +$$

$$\int_0^{P_s}\delta\ln q\left[(a(P_s)B_s - b(P_s)B_a + c(P_s)B_a)\tau_s + b(P_s)\int_P^{P_s}\tau dB + c(P_s)\left(\int_P^{P_s}\tau^*dB - 2\int_0^{P_s}\tau^*dB\right)\right]\frac{\partial\ln\tau_w}{\partial P}dP$$

$$= W_{T_s}(P_s)\delta T_s + \int_0^{P_s}W_T(P_s)\frac{\partial B}{\partial T}\delta TdP + \int_0^{P_s}W_q(P_s)\delta\ln q dP$$

where

$$W_{T_s}(P_s) = a(P_s)\tau_s\frac{\partial B_s}{T_s}$$

$$W_T(P_s) = \frac{\partial B}{\partial T}\left(b(P_s)\frac{\partial\tau}{\partial P} - c(P_s)\frac{\partial\tau^*}{\partial P}\right)$$

$$W_q(P_s) = \left[(a(P_s)B_s - b(P_s)B_a + c(P_s)B_a)\tau_s + b(P_s)\int_P^{P_s}\tau dB + c(P_s)\left(\int_P^{P_s}\tau^*dB - 2\int_0^{P_s}\tau^*dB\right)\right]\frac{\partial\ln\tau_w}{\partial P}$$

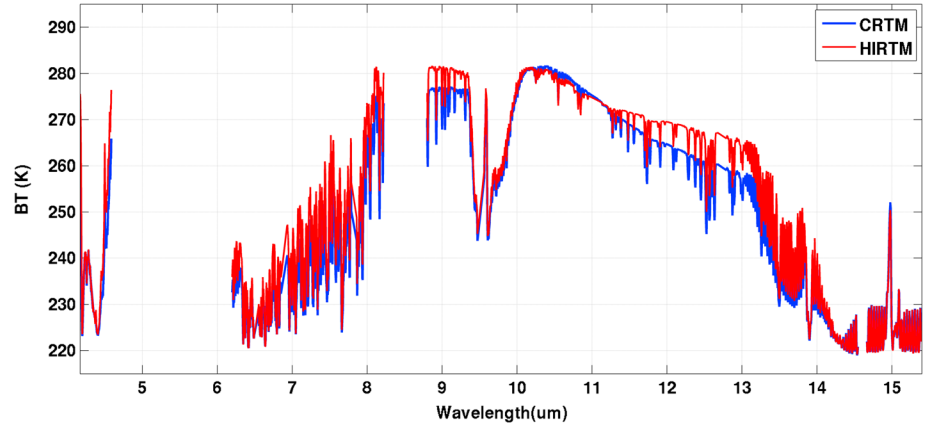Following the above procedure, we have

Figure 2. The AIRS BT calculations from HIRTM and CRTM with a COT of 1.0 and CTP of 300 hPa under ice cloud situations. The U.S. Standard Atmosphere is used in the calculations. Nadir view is assumed.

$$\delta R(P_c) = a(P_c)\tau_c\frac{\partial B_c}{T_c}\delta T_c + \int_0^{P_c}\frac{\partial B}{\partial T}\delta T d(b(P_c)\tau - c(P_c)\tau^*)$$

$$+ \int_0^{P_c}\delta\ln q\left[(a(P_c)B_c - b(P_c)B_c + c(P_c)B_c)\tau_c + b(P_c)\int_P^{P_c}\tau dB + c(P_c)\left(\int_P^{P_c}{}^\sim\tau^* dB - 2\int_0^{P_c}{}^\sim\tau^* dB\right)\right]d\ln\tau_w$$

$$= W_{T_c}(P_c)\delta T_c + \int_0^{P_c}W_T(P_c)\frac{\partial B}{\partial T}\delta T dP + \int_0^{P_c}W_q(P_c)\delta\ln q dP$$

$$\tag{22}$$

where

$$W_{T_s}(P_s) = a(P_s)\tau_s\frac{\partial B_s}{T_s}$$

$$W_T(P_s) = \frac{\partial B}{\partial T}\left(b(P_s)\frac{\partial\tau}{\partial P} - c(P_s)\frac{\partial\tau^*}{\partial P}\right)$$

$$W_q(P_s) = \left[(a(P_s)B_s - b(P_s)B_a + c(P_s)B_a)\tau_s + b(P_s)\int_P^{P_s}\tau dB + c(P_s)\left(\int_P^{P_s}\tau^* dB - 2\int_0^{P_s}\tau^* dB\right)\right]\frac{\partial\ln\tau_w}{\partial P}$$

The above three terms are Jacobians for surface skin temperature, temperature, and moisture profiles in cloudy regions. The Jacobians of the cloud parameters (cloud top pressure, cloud particle size, and cloud optical thickness) can be derived via the numerical perturbation method [*Li et al.*, 2005]. Using geometric assumptions (e.g., effective cloud emissivity and cloud top pressure), the Jacobians of cloud parameters can also be derived analytically [*Li et al.*, 2001].
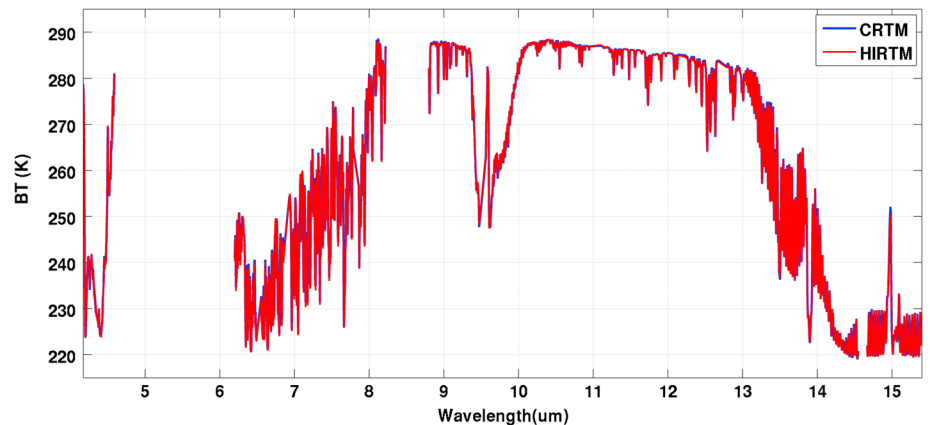

Figure 3. The AIRS BT calculations from HIRTM and CRTM with a COT of 1.0 and CTP of 700 hPa under water cloud situations. The U.S. Standard Atmosphere is used in the calculations. Nadir view is assumed.
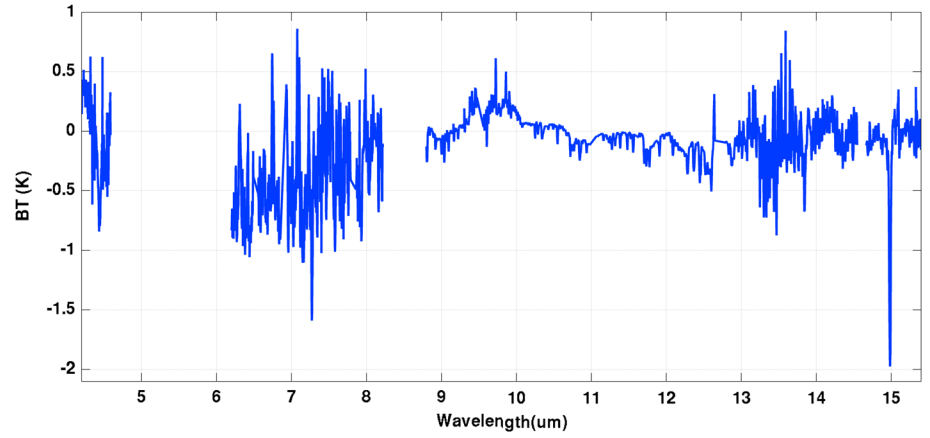
Figure 4. Clear-sky AIRS BT differences (HIRTM − CRTM) calculated from U.S. Standard Atmosphere. Surface emissivity was set to 0.95 for all channels, CO_2 was set to 380 ppmv, and the surface pressure was set to 1000 hPa; nadir view was assumed in the calculations.

In clear-sky situations, $a = \varepsilon_s$, $b = 1$, and $c = (1 − \varepsilon_s)$, we have

$$\delta R = \varepsilon_s \tau_s \delta B_s + \int_0^{P_s} \delta B \mathrm{d}(\tau − (1 − \varepsilon_s)\tau^*) + \int_0^{P_s} \delta \ln q \left[\varepsilon_s(B_s − B_a)\tau_s + \int_P^{P_s} \tau \mathrm{d}B + (1 − \varepsilon_s)\left(\int_P^{P_s} \tau^* \mathrm{d}B − 2\int_0^{P_s} \tau^* \mathrm{d}B \right) \right] \mathrm{d}\ln\tau_w$$

$$= \varepsilon_s \tau_s \delta B_s − \int_0^{P_s} \delta B \mathrm{d}[\tau − (1 − \varepsilon_s)\tau^*] + \int_0^{P_s} \delta \ln q \left\{ \varepsilon_s(B_s − B_a)\tau_s + \int_P^{P_s}[\tau + (1 − \varepsilon_s)\tau^*]\mathrm{d}B − 2(1 − \varepsilon_s)\int_0^{P_s} \tau^* \mathrm{d}B \right\} \mathrm{d}\ln\tau_w$$
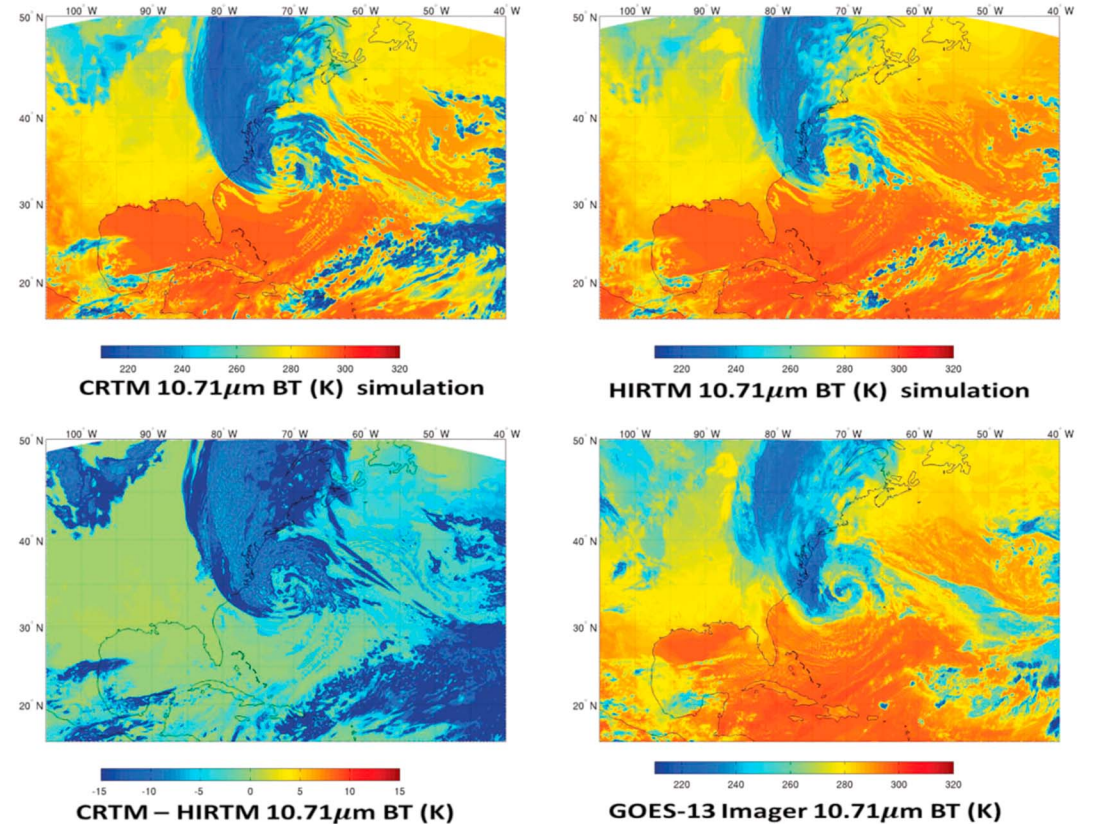
$$(23)$$

or

Figure 5. The simulated GOES 13 Imager 10.71 µm brightness temperatures (BTs) from (top left) CRTM, (top right) HIRTM, (bottom right) the observations, and the (bottom left) BT differences between CRTM and HIRTM.
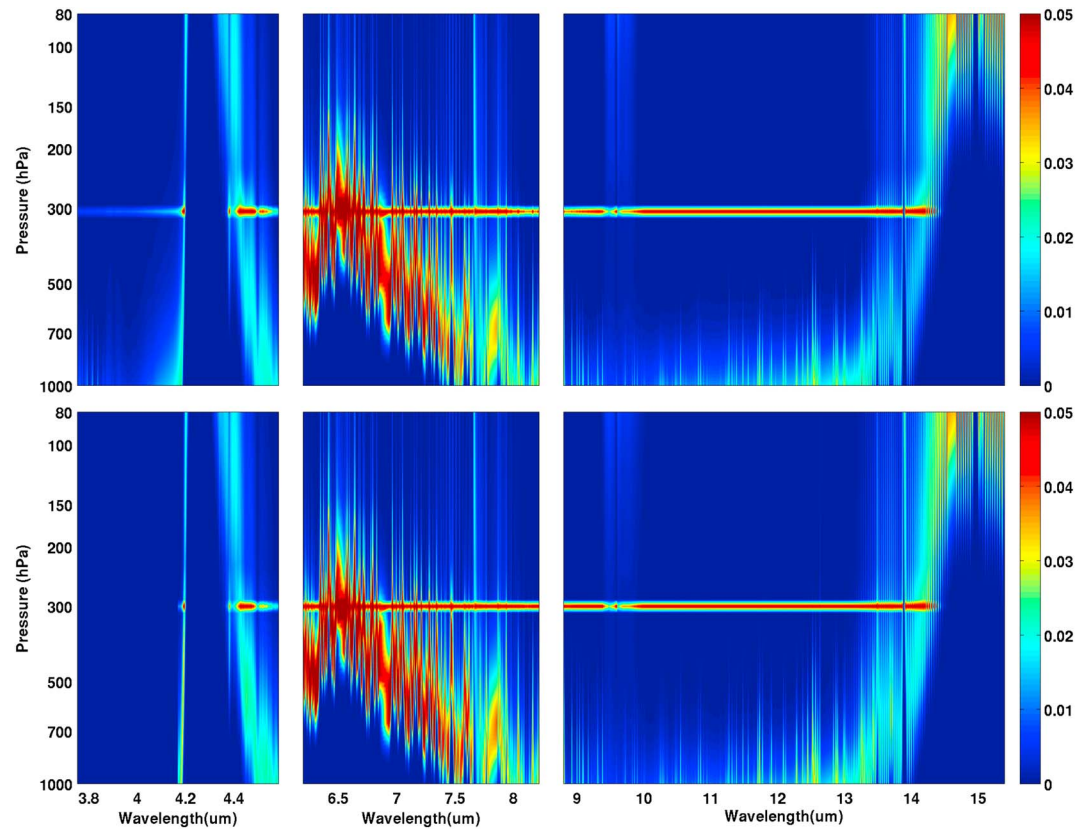
Figure 6. The temperature Jacobians of AIRS for an ice cloudy case with CTP of 300 hPa and COT of 0.5. The U.S. Standard Atmospheric profile with nadir view is used in the calculations. (top row) For CRTM. (bottom row) For HIRTM.

$$\delta R = a\tau_s \delta B_s + \int_0^{P_s} \delta B \mathrm{d}(b\tau - c\tau^*) + \int_0^{P_s} \delta \ln q \left[(aB_s - bB_a + cB_a)\tau_s + \int_P^{P_s}(b\tau - c\tau^*)\mathrm{d}B - 2c\int_P^{P_s}\tau^*\mathrm{d}B \right] \mathrm{d}\ln\tau_w \quad (24)$$

Those clear-sky Jacobian forms can be used for retrieval and data assimilation if only clear IR radiances are used.

4. BT Comparison With CRTM

Comparisons between HIRTM and CRTM have been conducted under cloudy skies. In the simulation, the U.S. standard atmosphere is used with an artificial cloud assumption for ice and water cloud situations. Figure 2 shows AIRS BTs from HIRTM and CRTM with a COT of 1.0 and cloud top pressure (CTP) of 300 hPa; a nadir view is assumed in the calculations. For HIRTM, cloud location is set at a pressure level of 300 hPa, with a cloud particle effective diameter of 10 μm and COT of 1.0; in the CRTM calculations, the cloud location was set at a layer ranging from 300 hPa to 314.136936 hPa, the cloud particle size (CPS) effective radius was set to 5 μm, and the cloud water content was set to 0.002784223 kg/m^2 (equivalent to a COT of 1.0 at 550 nm). While HIRTM and CRTM agree with each other in the absorption IR spectral regions, CRTM is colder (about 2–7 K) in the IR window regions for this ice cloud case. Figure 3 is the same as Figure 2 but for a water cloud with a CTP of 700 hPa and cloud particle diameter of 20 μm. The cloud in CRTM is set accordingly to ensure consistency. The HIRTM and CRTM agree well in both the absorption and window IR spectral regions under water clouds, with a BT difference usually less than 1.0 K. It should be noted that the clear-sky BT differences between different RTMs are small (less than 0.5 K for the majority of spectral bands, see Figure 4 for clear-sky BT differences). So the large differences between HIRTM and CRTM in ice cloud conditions are mainly caused by the differences in the cloud model.

A CRTM cold bias for ice clouds has been also reported by Greenwald (personal communication, 2017) and Otkin (personal communication, 2017) of the Cooperative Institute for Meteorological Satellite Studies at the University of Wisconsin-Madison.
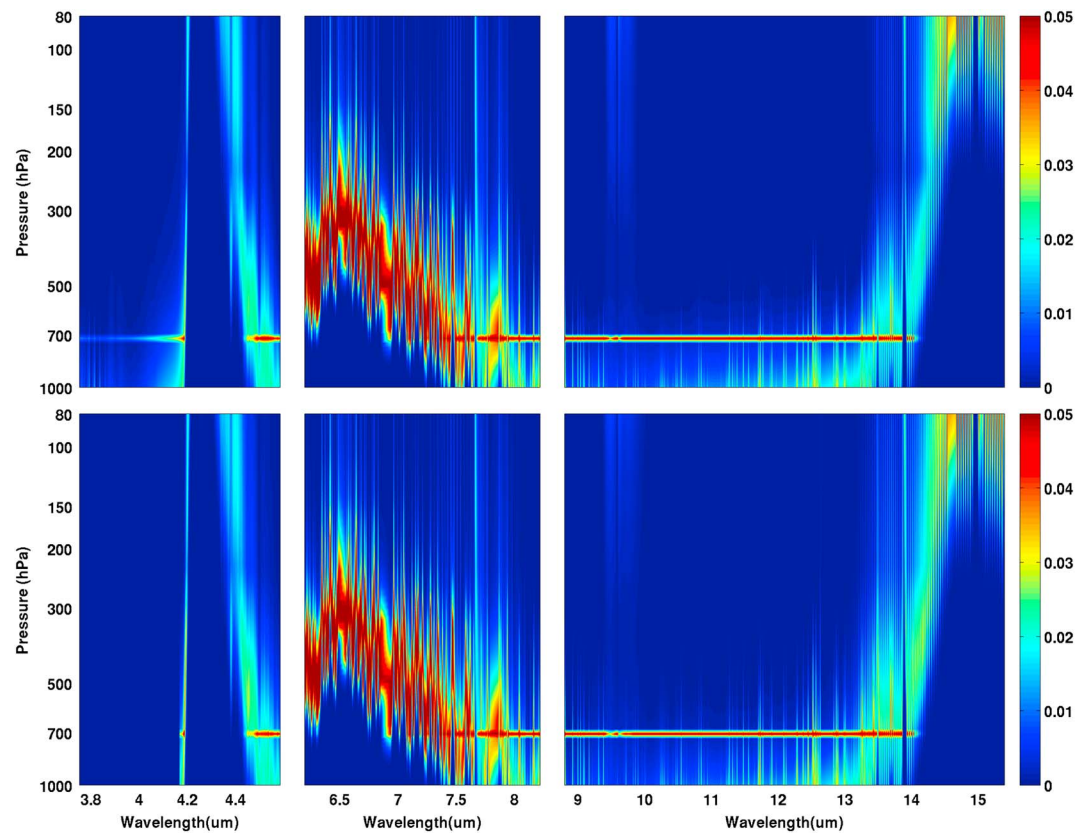
Figure 7. The temperature Jacobians of AIRS for a water cloud case with CTP of 700 hPa and COT of 0.5. The U.S. Standard Atmospheric profile with nadir view is used in the calculations. (top row) For CRTM. (bottom row) For HIRTM.

Figure 5 shows the simulated GOES 13 Imager 10.71 μm BTs from CRTM (top left) and HIRTM (top right), along with the observations (bottom right). The BT differences between CRTM and HIRTM are also shown in Figure 5 (bottom left). The 36 h forecast for 18 UTC 27 October 2012 from Weather Research and Forecasting (WRF) output for the Hurricane Sandy (2012) case is used in the calculations [*Wang et al.*, 2014, 2015]. When simulating cloudy radiances using HIRTM, it is critical to have an accurate cloud top pressure, which can be estimated from cloud hydrometer profiles. For example, one could determine the cloud top at the level where the integrated COT from the TOA (top of atmosphere) is greater or equal to a threshold (i.e., 0.1). However, this model is not reasonable enough because IR radiation can penetrate clouds, depending on the channels.
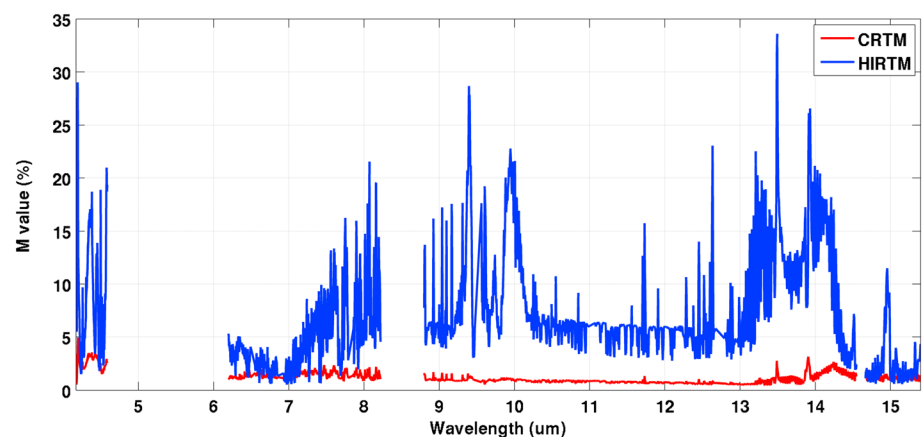

Figure 8. The *M* values of the temperature Jacobians for both HIRTM and CRTM. An ice cloud is assumed with a CTP of 300 hPa and COT of 0.5. The U.S. Standard Atmosphere with nadir view is assumed in the calculations.
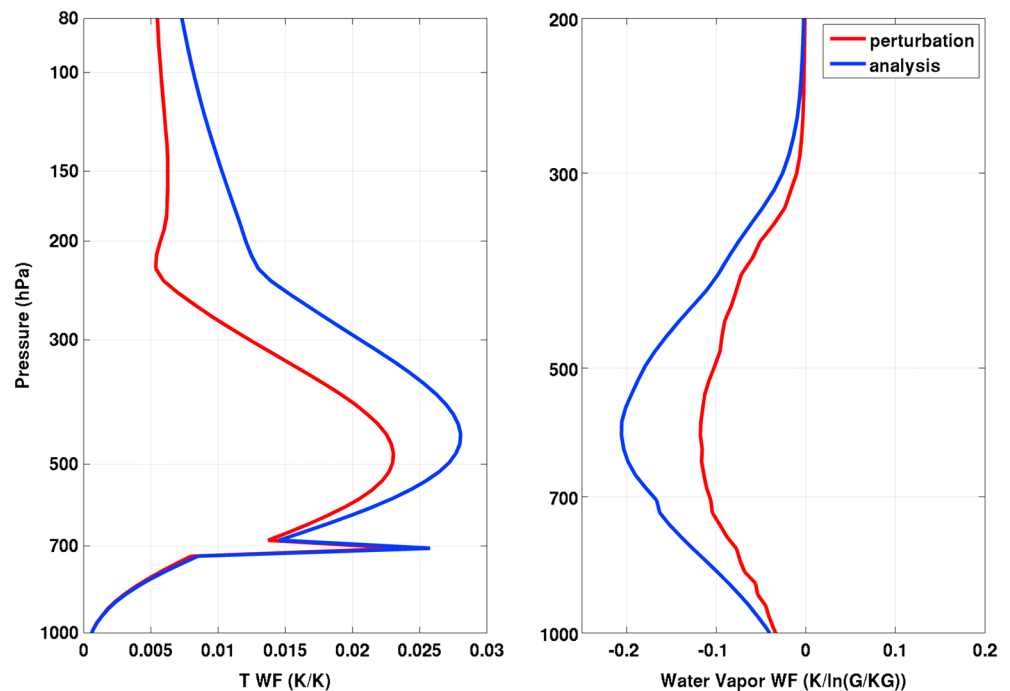
Figure 9. (left) Temperature Jacobians of AIRS channel number 210 with wavelength of 14.0962 μm and *M* value of 36. (right) Water vapor mixing ratio Jacobians of AIRS channel number 1392 with wavelength of 7.7094 μm and *M* value of 65. Both are for water cloud, CPS = 10 μm in dimeter, COT = 0.5, and CTP = 700 hPa.

In addition, this method might cause problems for thin cirrus clouds on top of water clouds because much of the contribution to the observed radiances is coming from below the cirrus clouds. Assigning the cloud top at the cirrus cloud height will eliminate the contribution below the cirrus clouds, causing a significant cold bias in the simulated radiances. Instead, an effective cloud top is determined using a weighted average of all cloud layers. The weight of each layer is the transmittance change of that layer. This method is more physically sound because the effective cloud top will bring the cloud top closer to the water clouds beneath. As a result, the simulated radiances will not be unrealistically cold.

In clear and water cloudy situations, the CRTM and HIRTM agree very well and are also close to the observations. However, in thick ice cloudy situations (hurricane region), the differences between CRTM and HIRTM are significant with CRTM much colder than HIRTM, which is consistent with single profile calculations (Figures 2 and 3). HIRTM is closer to the GOES Imager observations in the hurricane region for this particular case. Further investigation into which key parameter or parameters is causing large differences between CRTM and HIRTM in thick ice cloudy simulations is needed.

5. Jacobian Comparisons With CRTM

The Jacobian (first derivative of the brightness temperature to an atmospheric parameter) calculations are also compared between HIRTM and CRTM. Figure 6 shows the temperature Jacobians of AIRS for an ice cloudy case with a cloud top pressure of 300 hPa and a COT of 0.5. Figure 6 (top row) is for CRTM, and Figure 6 (bottom row) is for HIRTM. Figure 7 is the same as Figure 6 but for a water cloud situation. In the calculations, the U.S. Standard Atmosphere with nadir view is assumed in both Figures 6 and 7.

In general, the temperature Jacobians from the two models agree with each other reasonably well from Figures 6 and 7. It should be noted that the cloud absorption and scattering model is only effective at spectral regions with wavelengths larger than 4.0 μm. Therefore, the Jacobians are not computed in the comparison for those channels with wavelengths less than 4.0 μm. In order to further evaluate the Jacobian calculations, an evaluation method described by *Garand et al.* [2001] was adapted, in which a goodness of fit measure, *M*, was defined as
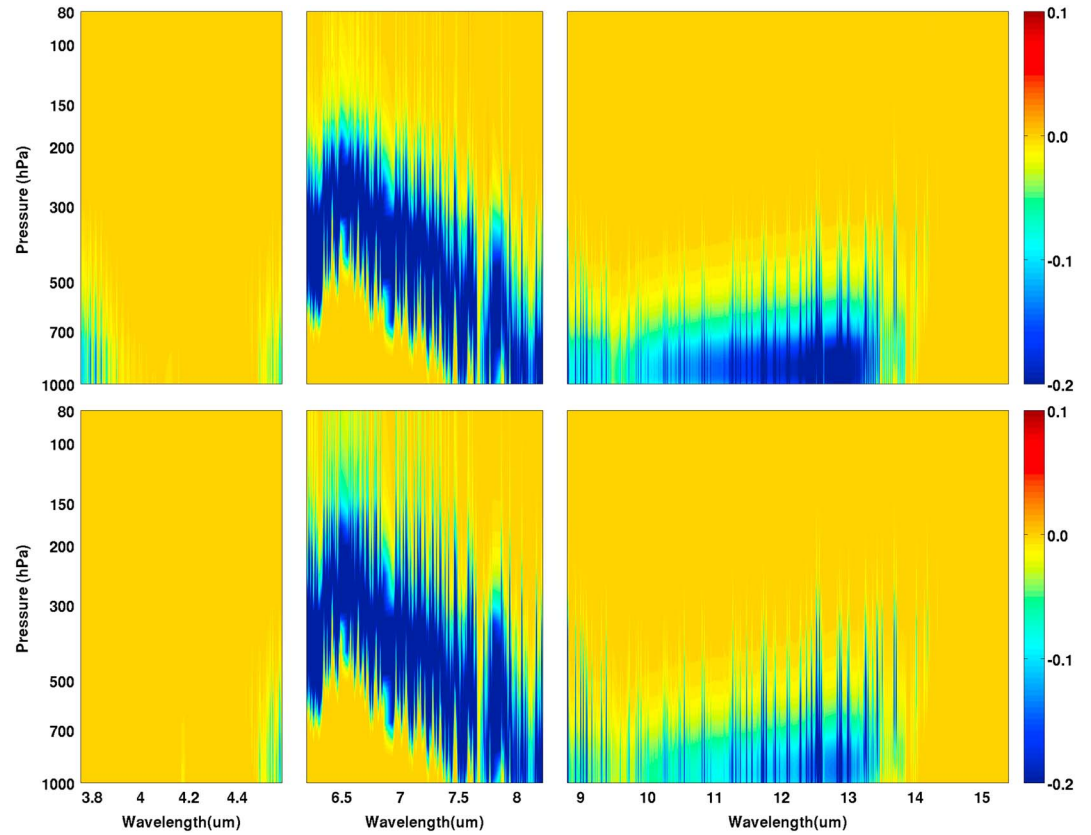
Figure 10. AIRS water vapor mixing ratio Jacobians calculation with water cloud (CTP = 700 hPa, cloud particle diameter = 10 μm, COT = 0.5). (top row) CRTM. (bottom row) HIRTM.

$$M = 100 \sqrt{\sum_{i=1}^{L} \left(J_{m,i} - J_{r,i} \right)^2 / \sum_{i=1}^{L} J_{r,i}^2}$$

where $J_{m,i}$ is the Jacobian of an atmospheric parameter at pressure level i for the RTM to be evaluated and $J_{r,i}$ is the Jacobian of an atmospheric parameter at pressure level i, used as a reference. $J_{r,i}$ is calculated using a perturbation method which is considered accurate but slows

$$J(x) = \frac{R\left(x + \frac{1}{2}\delta x\right) - R\left(x - \frac{1}{2}\delta x\right)}{\delta x}$$

The perturbations used to calculate temperature and moisture Jacobians are 1 K and 1% respectively. Further decreasing perturbations have little impact on the calculated Jacobians. Smaller M values indicate more accurate calculations of the Jacobians. Figure 8 shows the M values of temperature Jacobians for both HIRTM and CRTM. Note that the Jacobian reference is calculated from its own model, which means the references for HIRTM and CRTM might have differences [*Jin et al.*, 2011].

For CRTM, the M values are very small. Since CRTM uses an adjoint method (fast and accurate) for the Jacobian calculations, the results should be very close to those calculated from the perturbation method. For HIRTM, the M values are within a reasonable range in most spectral regions, which is consistent with the results from *Garand et al.* [2001]. The M values from HIRTM in the 13.3–14.3 μm regions and near the 10 μm region are slightly large but still less than 40. The large M values in those spectral regions might be attributed to relatively large BT differences between the two models (see Figure 4), as well as the fact that HIRTM uses an analytical form which is an approximation assumption. Although the M values are relatively large for some channels, the shapes are similar between HIRTM and CRTM (see Figure 9), which should be fine for using the analytical form in both retrieval and radiance assimilation since the results are determined by weighting functions, the background covariance matrices, and observation errors. The tuning of the

background covariance matrix makes it less dependent on weighting functions [*Li and Huang*, 1999]. In applications, those M values can be used for channel selection, for example, using only channels with M values less than 20. It should be noted that the Jacobian calculations in HIRTM are much faster than those in CRTM since HIRTM uses the analytical form.

For the water vapor mixing ratio (in terms of $\ln q$) Jacobians, CRTM and HIRTM are very close in the strong water vapor absorption region, but in the window region or the weak absorption region, the differences are substantial. Figure 10 shows the water vapor mixing ratio (in terms of $\ln q$) Jacobians with a water cloud assumption.

6. Summary

An efficient radiative transfer model called HIRTM along with its linearization under cloudy-sky conditions has been developed for hyperspectral infrared radiance simulation, assimilation, and retrieval processing. It couples the atmospheric transmittance for molecule absorption and single scattering for cloud absorption and scattering. HIRTM and its analytical Jacobian have been compared with the CRTM; HIRTM and CRTM have similar BT calculations under water cloud situations while CRTM is substantially colder in ice cloud situations. Both have similar Jacobian calculations, and the M values of the Jacobian matrix for CRTM are a little smaller than those of HIRTM. However, because HIRTM uses the analytical form, its calculations are much faster than those from CRTM. Comparisons with GOES Imager observations also indicate that both perform similarly under water clouds, while CRTM has a cold bias for ice clouds.

HIRTM has been used in the retrieval process and has shown to be a very useful science package for quickly extracting cloud and atmospheric parameters for real-time applications. The purpose of developing HIRTM is not to replace CRTM in operational use, rather, through intercomparisons between CRTM and HIRTM in cloudy skies, CRTM might be improved in some situations (e.g., cold cloud scene as mentioned above) by better cloud parameterization (e.g., better conversion of NWP cloud hydrometer parameters to optical properties used by CRTM). Future work will be focused on applying HIRTM to directly assimilate IR cloudy radiances into a NWP model, as well as development of HIRTM accounting for the multilayer cloud effects.

References

Cardinali, C. (2009), Monitoring the observation impact on the short-range forecast, *Q. J. R. Meteorol. Soc.*, *135*, 239–250.
Chahine, M. T., et al. (2006), AIRS: Improving weather forecasting and providing new data on greenhouse gases, *Bull. Am. Meteorol. Soc.*, 911–926.
Cintineo, R., J. Otkin, M. Xue, and F. Kong (2014), Evaluating the performance of planetary boundary layer and cloud microphysical parameterization schemes in convection-permitting ensemble forecasts using synthetic GOES-13 satellite observations, *Mon. Weather Rev.*, *142*, 163–182.
Gambacorta, A., and C. Barnet (2013), Methodology and information content of the NOAA NESDIS operational channel selection for the Cross-Track Infrared Sounder (CrIS), *IEEE Trans. Geosci. Remote Sens.*, *51*, 3207–3216.
Garand, L., et al. (2001), Radiance and Jacobian intercomparison of radiative transfer models applied to HIRS and AMSU channels, *J. Geophys. Res.*, *106*, 24,017–24,031.
Greenwald, T., B. Pierce, T. Schaack, J. Otkin, M. Rogal, K. Bah, A. Lenzen, J. P. Nelson, J. Li, and H.-L. Huang (2016), Real-time simulation of the GOES-R ABI for user readiness and product evaluation, *Bull. Am. Meteorol. Soc.*, *97*, 245–261.
Hannon, S., L. L. Strow, and W. W. McMillan (1996), Atmospheric infrared fast transmittance models: A comparison of two approaches, in *Optical Spectroscopic Techniques and Instrumentation for Atmospheric and Space Research II*, *International Society for Optical Engineering* vol. 2830, edited by P. B. Hays and J. Wang, pp. 94–105.
Heilliette, S., and L. Garand (2007), A practical approach for the assimilation of cloudy infrared radiances and its evaluation using airs simulated observations, *Atmos. Ocean*, *45*(4), 211–225, doi:10.3137/ao.450403.
Huang, H.-L., L. E. Gumley, K. Strabala, J. Li, E. Weisz, T. Rink, K. Baggett, J. E. Davies, W. L. Smith, and J. C. Dodge (2004), International MODIS and AIRS Processing Package (IMAPP): A direct broadcast software for the NASA Earth observing system, *Bull. Am. Meteorol. Soc.*, *85*, 159–161.
Jiang, X. W. (2016), Evaluation of environmental moisture from NWP models with measurements from advanced geostationary satellite imager, MS thesis, 53 pp., Univ. of Wisconsin-Madison.
Jin, X., J. Li, T. Schmit, and M. Goldberg (2011), Evaluation of radiative transfer models in atmospheric profiling with broadband infrared radiance measurements, *Int. J. Remote Sens.*, *32*, 863–874.
Karagulian, F., L. Clarisse, C. Clerbaux, A. J. Prata, D. Hurtmans, and P.-F. Coheur (2010), Detection of volcanic SO_2 ash, and H_2SO_4 using the Infrared Atmospheric Sounding Interferometer (IASI), *J. Geophys. Res.*, *115*, D00L02, doi:10.1029/2009JD012786.
Kelly, G., and J.-N. Thepaut (2007), Evaluation of the impact of the space component of the global observation system through observing system experiments, ECMWF Newsletter, No. 113, pp. 16–28, ECMWF, Reading, U. K. [Available online at http://www.ecmwf.int/publications/newsletters/pdf/113.pdf.]
Le Marshall, J., et al. (2005), AIRS hyperspectral data improves Southern Hemisphere forecasts, *Aust. Meteorol. Mag.*, *54*, 57–60.
Le Marshall, J., et al. (2006), Improving global analysis and forecasting with AIRS, *Bull. Am. Meteorol. Soc.*, *87*, 891–894.

Li, J. (1994), Temperature and water vapor weighting functions from radiative transfer equation with surface emissivity and solar reflectivity, *Adv. Atmos. Sci.*, *11*, 421–426.

Li, J., and H.-L. Huang (1999), Retrieval of atmospheric profiles from satellite sounder measurements by use of the discrepancy principle, *Appl. Opt.*, *38*(6), 916–923.

Li, J., and J. Li (2008), Derivation of global hyperspectral resolution surface emissivity spectra from advanced infrared sounder radiance measurements, *Geophys. Res. Lett.*, *35*, L15807, doi:10.1029/2008GL034559.

Li, J., F. X. Zhou, and Q. C. Zeng (1994), Simultaneous non-linear retrieval of atmospheric temperature and absorbing constituent profiles from satellite infrared sounder radiances, *Adv. Atmos. Sci.*, *11*, 128–138.

Li, J., W. Wolf, W. P. Menzel, W. Zhang, H.-L. Huang, and T. H. Achtor (2000), Global soundings of the atmosphere from ATOVS measurements: The algorithm and validation, *J. Appl. Meteorol.*, *39*, 1248–1268.

Li, J., W. P. Menzel, and A. J. Schreiner (2001), Variational retrieval of cloud parameters from GOES sounder longwave cloudy radiance measurements, *J. Appl. Meteorol.*, *40*, 312–330.

Li, J., W. P. Menzel, F. Sun, T. J. Schmit, and J. Gurka (2004), AIRS subpixel cloud characterization using MODIS cloud products, *J. Appl. Meteorol.*, *43*, 1083–1094.

Li, J., H.-L. Huang, C.-Y. Liu, P. Yang, T. J. Schmit, H. Wei, E. Heli, L. G. Weisz, and W. P. Menzel (2005), Retrieval of cloud microphysical properties from MODIS and AIRS, *J. Appl. Meteorol.*, *44*, 1526–1543.

Li, J., J. Li, E. Weize, and D. K. Zhou (2007), Physical retrieval of surface emissivity spectrum from hyperspectral infrared radiances, *Geophys. Res. Lett.*, *34*, L16812, doi:10.1029/2007GL030543.

Li, J., P. Wang, H. Han, J. Li, and J. Zheng (2016), On the assimilation of satellite sounder data in cloudy skies in the numerical weather prediction models, *J. Meteorol. Res.*, *30*, 169–182.

Li, Z., J. Li, W. P. Menzel, T. J. Schmit, J. P. Nelson, III, J. Daniels, and S. A. Ackerman (2008), GOES sounding improvement and applications to severe storm nowcasting, *Geophys. Res. Lett.*, *35*, L03806, doi:10.1029/2007GL032797.

Li, Z., J. Li, W. P. Menzel, J. P. Nelson, T. J. Schmit, E. Weisz, and S. Ackerman (2009), Forecasting and nowcasting improvement in cloudy regions with high temporal GOES sounder infrared radiance measurements, *J. Geophys. Res.*, *114*, 2009, doi:10.1029/2008JD10596.

Smith, W. L., H. Revercomb, G. Bingham, A. Larar, H. Huang, D. Zhou, J. Li, X. Liu, and S. Kireev (2009), Evolution, current capabilities, and future advance in satellite ultra-spectral IR sounding, *Atmos. Chem. Phys. Discuss.*, *9*, 1–29.

Smith, W. L., E. Weisz, S. Kireev, D. Zhou, Z. Li, and E. Borbas (2012), Dual-regression retrieval algorithm for real-time processing of satellite ultraspectral radiances, *J. Appl. Meteorol. Climatol.*, *51*, 1455–1476.

Smith, N., W. L. Smith, E. Weisz, and H. E. Revercomb (2015), AIRS, IASI, and CrIS retrieval records at climate scales: An investigation into the propagation of systematic uncertainty, *J. Appl. Meteorol. Climatol.*, *54*, 1465–1481.

Strow, L. L., S. E. Hannon, S. DeSouza-Machado, H. Motteler, and D. Tobin (2003), An overview of the AIRS radiative transfer model, *IEEE Trans. Geosci. Remote Sens.*, *41*, 303–313.

Susskind, J., C. D. Barnet, and J. M. Blaisdell (2003), Retrieval of atmospheric and surface parameters from AIRS/AMSU/HSB under cloudy conditions, *IEEE Trans. Geosci. Remote Sens.*, *41*, 390–409.

Wang, P., J. Li, J. Li, Z. Li, T. J. Schmit, and W. Bai (2014), Advanced infrared sounder subpixel cloud detection with imagers and its impact on radiance assimilation in NWP, *Geophys. Res. Lett.*, *41*, 1773–1780, doi:10.1002/2013GL059067.

Wang, P., J. Li, M. Goldberg, T. J. Schmit, A. H. N. Lim, Z. Li, H. Han, J. Li, and S. A. Ackerman (2015), Assimilation of thermodynamic information from advanced IR sounders under partially cloudy skies for regional NWP, *J. Geophys. Res. Atmos.*, *120*, 5469–5484, doi:10.1002/2014JD022976.

Wei, H., P. Yang, J. Li, B. A. Baum, H.-L. Huang, S. Platnick, Y. Hu, and L. Strow (2004), Retrieval of semitransparent ice cloud optical thickness from Atmospheric Infrared Sounder (AIRS) measurements, *IEEE Trans. Geosci. Remote. Sens.*, *42*, 2254–2267.

Weisz, E., J. Li, D. K. Zhou, H.-L. Huang, M. D. Goldberg, and P. Yang (2007), Cloudy sounding and cloud-top height retrieval from AIRS alone single field-of-view radiance measurements, *Geophys. Res. Lett.*, *34*, L12802, doi:10.1029/2007GL030219.

Weisz, E., W. L. Smith, and N. Smith (2013), Advances in simultaneous atmospheric profile and cloud parameter regression based retrieval from high-spectral resolution radiance measurements, *J. Geophys. Res. Atmos.*, *118*, 6433–6443, doi:10.1002/jgrd.50521.

Weisz, E., N. Smith, and W. L. Smith (2015), The use of hyperspectral sounding information to monitor atmospheric tendencies leading to severe local storms, *Earth and Space Science*, *2*, 369–377.

Wu, X., J. Li, W. P. Menzel, H. L. Huang, K. Bagget, and H. Revercomb (2005), Evaluation of AIRS cloud properties using MPACE data, *Geophys. Res. Lett.*, *32*, L24819, doi:10.1029/2005GL024400.

Yang, P., K. N. Liou, and P. W. Arnott (1997), Extinction efficiency and single-scattering albedo of ice crystals in laboratory and natural cirrus clouds, *J. Geophys. Res.*, *102*, 21,825–21,835.

Zhou, D., W. L. Smith, X. Liu, A. Larar, S. Mango, and H. Hung-Lung (2007), Physically retrieving cloud and thermodynamic parameters from ultraspectral IR measurements, *J. Atmos. Sci.*, *64*, 969–982.